Localized measurements of optical thickness variations in femtosecond trimmed structures

A. L. Lereu*, F. Lemarchand, and M. Lequime
Institut Fresnel UMR 6133 – Université Paul Cézanne - France

Currently, the utilization of high power ultrafast lasers to induce optical changes in structures for the purpose of locally drawing patterns with dimensions inferior to the diffraction limit is well-established and controlled. Using this technique, we aim to modify the refractive index and/or the geometrical parameters of an optical interferential filter composed of successive thin layers. This local optimization will then allow the improvement or tuning of the performances of the optical filters. Thereafter, it is necessary to characterize these local modifications to achieve the final response of the expected filter. In our work, we developed a dedicated optical system, based on Fabry-Perot interferometry, to measure optical thickness, ranging from 10^{-3} to 10^{-4}, with a high spatial resolution (in the order of 5x5µm). We present here our preliminary results carried out on calibrated test samples.
Keywords: Fabry-Perot interferometry, Refractive index variation, femtosecond laser trimming
* *Corresponding author: aude.lereu@fresnel.fr*

1- INTRODUCTION

The use of powerful lasers is now well established in the industry to perform marking, cutting, drilling or welding operations on a wide range of materials and parts [1]. The quality of this laser machining is driven by the geometrical characteristics of the focused light beam (the sharpness of the "laser tool") as well as by the heat exchange phenomena between the machined area and the surrounding zone. It is one of the reason for which excimer lasers (which emit in the near UV part of the spectrum) can provide in some cases very attractive solutions [2,3]. The recent development of high power ultrafast lasers [4] (delivering energetic pulses in the range of few micro-joules with a duration of about one hundred of femtoseconds) has permitted to drastically improve the quality of this micromachining, first by increasing the peak power of the laser tool (typically the giga-watt), second by limiting the diffusion of the deposited energy around the focal point (the duration of the laser pulse is indeed much shorter than the heat diffusion time inside the material) and third by involving highly non linear laser-matter interaction phenomena [5-7]. This deterministic character of optical damage produced by femtosecond laser pulses [8,9] can be used to machine patterns whose dimensions are far below the diffraction limit.

Obviously, the accuracy of this micro-machining is directly connected to the duration and energy stability of the used femtosecond laser pulses [10], but nowadays it seems possible to reach a reproducibility of few nanometers. Moreover, femtosecond laser pulses are also able, at lower fluence levels, to produce a localized change in the refractive index of transparent materials, which can be used to perform a direct laser writing of a waveguide in the bulk of a glass substrate [11-14] or to develop entirely new photonic device integration and fabrication procedures [15-17]. Besides, standard Nd:YAG lasers are today widely used in the semiconductors industry to adjust (or trim) thin film resistors or thin film capacitors to very tight electrical performance specifications [18,19], and to correct in this way imprecision in the deposition process. We therefore aim here to combine these different approaches (femtosecond laser micromachining of dielectric materials, localized refractive index changes induced by ultrafast laser and thin-film laser trimming) for an entirely new goal (to our knowledge), i.e. the optimization of the performances of optical interference coatings by femtosecond laser processing.

As an illustration of this approach, let us consider a narrow bandpass interference filter including two identical reflective stacks with 19 alternated low and high index quarter-wavelength layers surrounding a half-wavelength spacer layer: the spectral bandwidth of such a structure is about 0.5 nm for a maximum transmission close to 90%. The thickness of each layer and the one of the spacer slightly varies at the surface of the component (for instance 10^{-4} per millimeter in relative units), with a spatial dependence defined by a lot of parameters including not only the nature of the deposition process (for instance, ion beam sputtering) and some critical parameters (like the composition of the target or the energy of the

Optical Fabrication, Testing, and Metrology III, edited by Angela Duparré, Roland Geyl
Proc. of SPIE Vol. 7102, 710203 · © 2008 SPIE · CCC code: 0277-786X/08/$18 · doi: 10.1117/12.797415

sputtering ions), but also the geometrical characteristics of the vacuum chamber (and especially the position and the orientation of the substrate with respect to the sputtering target). As a consequence, the central wavelength of this filter is not uniform at the surface of the component: the use of a femtosecond laser source precisely focused inside the spacer could permit to cancel the effect of these thickness variations by acting on the local value of the refractive index of this layer.

In addition, the micro-machining ability of this femtosecond laser sources could also be utilized to engrave subwavelength periodic structures in the top layer of an antireflective stack: the presence of such a structure induces, at a specific wavelength, a very high efficiency coupling of the incident beam into guided modes of the stack and can be used to manufacture narrow notch filters with optimized angle and polarization behavior [20]. This machining ability can also be used to remove the coating from some specific areas of a uniform coated component, without any risk of degradation of the unprocessed zones and with very abrupt transitions between processed and unprocessed zones.

We present here a dedicated experimental setup in an attempt to reach a spatially localized measurement (imperfections of the deposition and/or defects of 5x5 µm) of refractive index variations as low as 10^{-4} over large samples. In Section 2, we numerically introduce the problem and evoke potential solutions. In Section 3, we describe our experimental setup and the calibrated samples employed to quantify the limitations of our apparatus, followed by the preliminary results and observations in Section 4, and a conclusion in Section 5.

2- SIMULATIONS

The determination of a small (typically 10^{-4}) refractive index variation for a dielectric thin layer with a thickness around 100 nm is not obvious. In general, photometric techniques, adapted to layer index determinations, consist in analyzing, over a large spectral range, the transmitted and reflected flows of a single coated layer (with a thickness of approximately 1 µm). Basically, one can observe spectral oscillations of these parameters and, then extract from this behavior the thickness and refractive index of the studied layer. Hence, the absolute precision for the refractive index real part is only around 10^{-2} [21]. Indeed, measuring transmittance and/or reflectance versus wavelengths is far more sensitive to the optical thickness (*nd*) (relative precision of about 10^{-3}) than to the individual evaluation of *n* and *d* (around 10 times less precise).

In our case, the problem is even more complex: a small index variation (from 10^{-2} to 10^{-4}) is expected over a thickness of 100 nm only. Obviously, such a small thickness is not sufficient to observe strong oscillations in the transmittance versus wavelengths. A direct photometric measurement is then inefficient. If we now consider a 1 µm thick layer with an index variation over only 100 nm thick; representing 10% of the layer thickness; spectral oscillations will clearly appear, however the resulting effect will be 10 times less intense, as only 10% of the layer is concerned and the other 90% stays purely homogeneous.

One solution consists in exalting the index variation (Δn) effect using Fabry-Perot cavities. These latter are resonant structures where two mirrors are deposited on both sides of the studied layer. This layer, also called "spacer layer", is then sandwiched inside the cavity, and therefore the electric field may undergo enhancements hundreds of times inside the spacer layer. The transmittance of these structures as a function of wavelengths (λ) is given by the following equation:

$$T = \frac{T_{\max}}{1 + F \sin^2 \varphi}$$

where $\boldsymbol{F}$ (the finesse of the cavity) , $\boldsymbol{T_{max}}$ (the maximum transmittance) and $\boldsymbol{\varphi}$ (the phase) can be written as

$$F = \frac{4\sqrt{R_1 R_2}}{(1-\sqrt{R_1 R_2})^2},\ T_{\max} = \frac{T_1 T_2}{(1-\sqrt{R_1 R_2})^2}, \text{ and } \varphi = \frac{2\pi}{\lambda} nd + \frac{\delta_1 + \delta_2}{2},$$

with R_1 and R_2 (respectively T_1 and T_2) the reflectance (resp. transmittance) of the two mirrors. δ_i with i=1,2 is the phase of the complex reflection amplitude coefficient r_i of each mirror. The resonance peaks of the structure appear then at discrete wavelengths when verifying $\varphi = 0$.

Considering now the case of a single coated layer, where tiny Δn imply small shifts of the wavelengths (λ) spectrum. Therefore, in order to be sensitive enough to slight Δn and consequently to small $\Delta\lambda$, it is mandatory to consider sharp resonance peaks. As a result, the finesse ***F*** of the cavity needs to be increased and the reflectivity of each mirror composing the cavity should approach 100%.

In addition, we recall (see [22]) that for a Fabry-Perot cavity with a homogenous structure the spectral shift ($\Delta\lambda$) can be linked with the variation of the optical thickness (Δnd) of the spacer by:

$$\frac{\Delta\lambda}{\lambda_0} = \kappa \frac{\Delta nd}{nd}$$

where κ is a factor depending on the structure that is equal to 1 in the best case. The relation between $\Delta\lambda$ and Δn can then be deducted from the equation above.

Moreover, in our case, the expected Δn is not over the whole thickness of the spacer layer, but only over 100 nm of the total thickness. Therefore, for a typical spacer thickness of 500 nm, the average effect of Δn is divided by 5. We can then assume that the relation between $\Delta\lambda$ and Δn can be expressed as

$$\Delta\lambda \approx \frac{\Delta n}{5n}\lambda_0 .$$

Numerically, a $\Delta n = 10^{-4}$ will cause a spectral shift below 10 pm for a central wavelength of 800 nm when considering the spacer layer exclusively. Such a spectral shift can merely be measured on very narrowband structures. Hence, we have considered two possible resonant structures: one with 17 layers mirrors (named structure A in Figs. 1a)) and one with 25 layers mirrors (named structure B in Figs. 1b)). In each configuration, the mirrors are made of an alternation of materials with refractive index of 2.1 and 1.45. The resulting reflectance in structure A and B is then estimated to be 99.75% and 99.99% respectively. We have moreover set for both cases, the parameters for the spacer layer to be 1.45 for the refractive index and 580 nm for the total thickness.

Finally, we have introduced a defect inside the spacer with a Δn of 10^{-4} and with a thickness of 100 nm. The calculated spectral shift is about 4 pm for both structures that is from an experimental point of view, difficult to evaluate. However, the peaks obtained for structure B are much sharper than for structure A, as seen in Fig. 1b), and therefore the shift might be measurable with a tunable laser source. Another possibility is to measure the transmittance as a function of the incident angle, the calculation, given in Figs. $1a_2$) and b_2), illustrates this behavior for the two structures, and will be experimentally used later in this work.

Structure A: Cavity with mirrors composed by 17 layers

Structure B: Cavity with mirrors composed by 25 layers

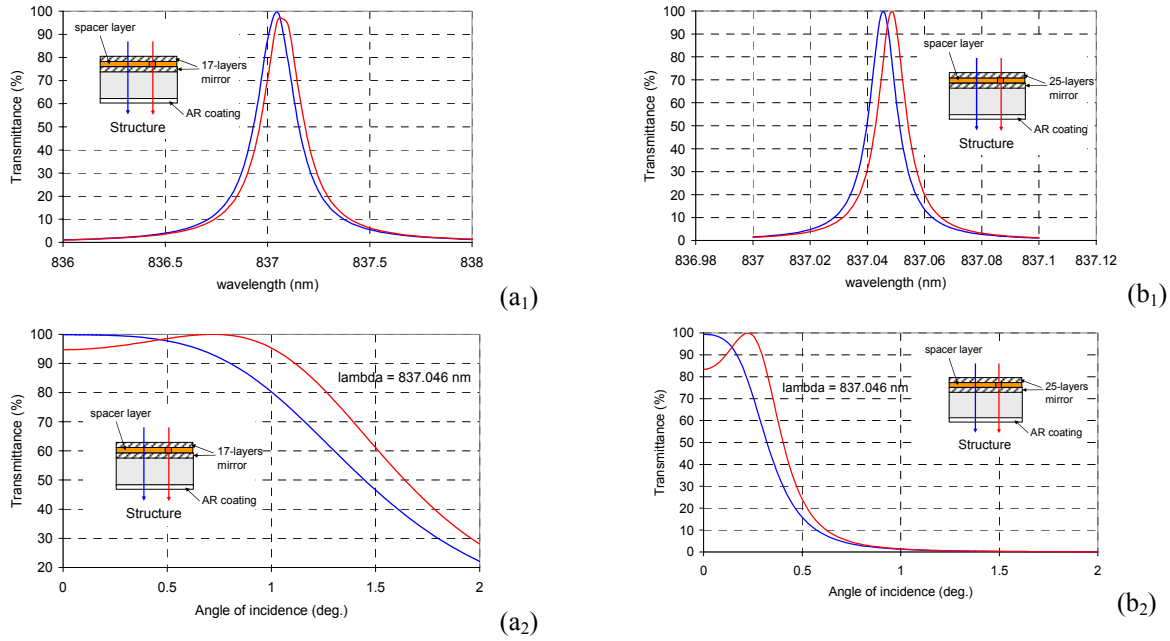

Fig. 1: Numerical predictions of the transmittance versus incident wavelengths (a_1 and b_1) and versus incident angles (a_2 and b_2) for two resonant structures in the infra-red spectral region. (a) for structure A with mirrors of 17 layers and (b) for structure B with mirrors of 25 layers.

3- EXPERIMENT

Our experimental setup, described in Fig. 2, can be used in two configurations, in order to either evaluate the transmittance variations (Fig. 2a)) or localize the microstructures (Fig. 2b)). However, for both configurations, the body of the experiment utilizes a laser source coupled into a collimator (coupling of 99%) and eventually into a lambdameter (coupling of 1%) to precisely control the wavelength variations. The collimator is designed for long distance projection applications with a wavefront error below λ/10 and a full beam divergence below 0.5 mrad. This permits to obtain a 5 mm collimated and uniform beam to illuminate the sample. The former is mounted on a precise xyz-stage allowing to select the region of interests of the sample. A charge-coupled detector (CCD) is then positioned, either directly behind the sample plan, in order to collect the transmittance (configuration of Fig. 2a)), or after a microscope objective to image the structures (Fig. 2b)). The CCD (PCO.1600 from Photon lines) resolution is expected to be 7.4x7.4 µm, with a time exposure interval between 5 µs and 60 seconds. The employed objective is chosen to be plan-apochromatic in order to limit geometric and spectral aberrations, as well as for its large numerical aperture (NA=0.42), its high working distance (WD=15 mm) and a magnification of 10x. The employed illumination sources are a large band infra-red source with a wavelength interval of 854±10 nm and a 632.8 nm Helium-Neon laser line.

Calibrated samples, in refractive index variations Δn and in structure size, are developed to qualify our experimental setup. The structure pattern is given in Fig. 3. The technique of ions implantation is used to obtain such samples. Ions of Titanium are here implanted with different doses to perform disparate local modifications, and therefore achieve various Δn belonging to the interval from 5.10^{-2} to 1.10^{-4}. Four samples with identical pattern and substrates are then made for four different Δn. The designed sample, represented in Fig. 3, is therefore composed by four series of five identical structures, and chromium marks (arrows) denote the *x*- and *y*-positions of the microstructures classified by size. The microstructures are conceived to be series of squares with edges of 100 µm, 30 µm, 10 µm and 5 µm, and with a

thickness of 100 nm to simulate the ultimate conditions used for the final optical components. Optical microscope images are taken, as shown in Fig. 4, to confirm the microstructures sizes. A small deviation is observed where the largest squares are measured to be 82 µm, and the smallest to be 4 µm (see Fig. 4).

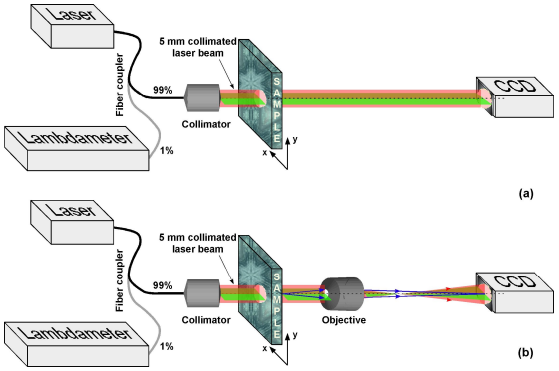

Fig. 2: Experimental setup for transmittance measurement. A laser beam is coupled into an optical coupler to be directed with 99% to a collimator and with 1% to a lambdameter in order to precisely control the wavelength variations. In configuration (a), the collimated beam of 5 mm of diameter illuminates the sample region of interest, and the signal is directly collected on a charge-coupled detector. In configuration (b), the transmitted signal is collected through a microscope objective, with a numerical aperture of 0.42, a working distance of 15 mm and a magnification of 10x. The sample in both configurations can be scanned in the *xyz*-directions to allow the transmittance measurement in every region.

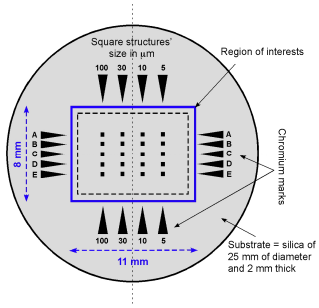

Fig. 3: Scheme of the calibrated samples. The technique of ions implantation is chosen to introduce local refractive index variations Δn. The modification is then carried out by adding ions of Titanium with different doses, ranging from 2.10^{16} Ti/cm^2 to 4.10^{13} Ti/cm^2, to create different Δn, ranging from 5.10^{-2} to 1.10^{-4}. The implantation is done in a depth of 100 nm in a 2 mm thick silica substrate, and the region of interests is limited to 8x11 mm. Marks of Chromium are appended to localize every structure.

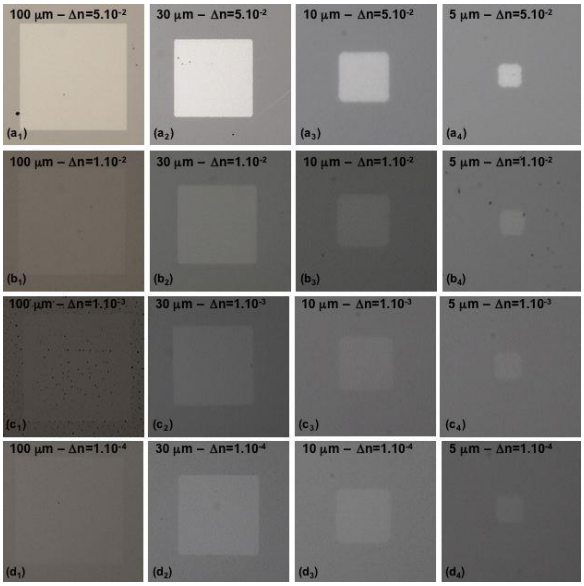

Fig. 4: Optical microscope images of four calibrated samples obtained as described in Fig. 3. The (a) series is for a $\Delta n=5.10^{-2}$, the (b) series for a $\Delta n=10^{-2}$, the (c) series for a $\Delta n=10^{-3}$ and the (d) series for a $\Delta n=10^{-4}$. A 20x objective is used to image the largest structures that are evaluated around 80 µm. The structures of series (2) are then obtained with a magnification of 50x and measured to be 30 µm. The last two series used a magnification of 100x and the sizes are estimated to be around 7 µm and 4 µm respectively.

Differential measurements are then carried out to eliminate background effects introduced by the substrate and the illumination source. Thereafter, we image the sample at two different places: without structures and with structures to be studied (see Figs. 5 and 6). The two images are collected one after the other in less than a second, or several images are taken in one position and the other to average potential variations.

4-RESULTS AND DISCUSSION

We present here first results obtained with two different illumination sources. Note that our numerical work in Section 2, considers an excitation source from 838 nm to 854 nm that will be the ultimate source we wish to use because of its spectral region but also its long coherence. Indeed, a long coherence enables a quasi monochromatic light emission, which is mandatory to expect detecting peak shift of about 1 to 10 pm (see Fig. 1). However, this long coherence introduces also additional interferences that parasites our measurements. This explains our choice here of a large band infra-red source with a wavelength interval of 854±10 nm (as used in Fig. 5) and a 632.8 nm Helium-Neon laser line (as used in Figs. 6 and 7), as mentioned in Section 3.

The same differential procedure is followed to obtain Figs. 5, 6 and 7, that is two successive images of two different regions of the sample are recorded. One (image 1 see Fig. 6a)) contains the structure under investigation and the other (image 2 see Fig. 6b)) the background information. After this first step, the ratio between image 1 and image 2 is carried out. The contrast around the structure is then improved; see Figs. 5, 6 and 7, as we eliminate potential effect introduced by the illumination source variations. In Figs. 5, 6 and 7, a 10x objective was used to resolve clearly every structure with size from 100x100 µm (Figs. 5b) and 6c)) down to 5x5 µm (Figs. 5d) and 7c)). Thanks to these preliminary images, we can conclude that one can resolve structures down to 5x5 µm with our system that was one of the requirements. In parallel, direct measurements, meaning without objective, were carried out to access to the real transmittance and therefore evaluate the exact Δn. Nevertheless, under these conditions, the spatial resolution is limited by the CCD camera resolution that is at the minimum 7.4x7.4 µm, and the working distances are extremely reduced, implying less flexibility for this configuration. Therefore, we kept the objective and measured the transmittance as a function incident angle by changing the angle from the sample plan (see Fig. 8). We observe expected oscillations of the transmittance as the incident angle is changed for two regions of the sample, i.e. without and with structure.

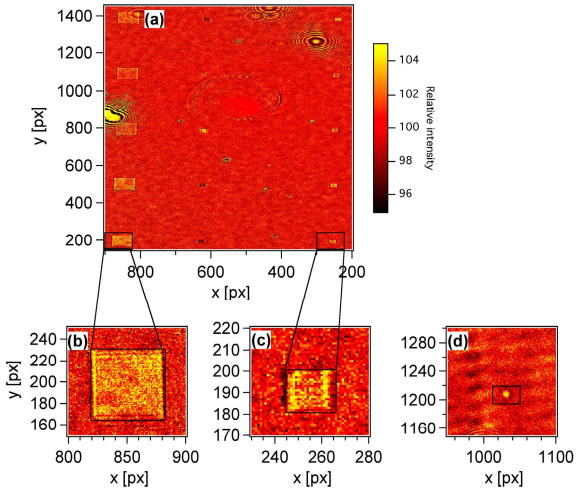

Fig. 5: Images resulting from the ratio of an image with structure over the background image with the broad band infra-red source and a 10x magnification. Image (a) shows the overall view of the region of interest, where the images (b) and (c) represent a zoom on the 100x100 µm and 30x30 µm structures observed in (a). In (d), we show that a defect of 5x5 µm may be resolved with this setup.

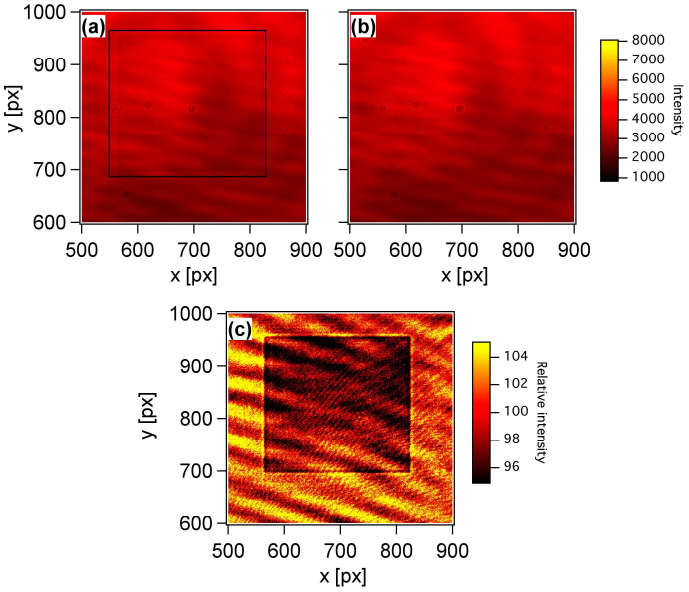

Fig. 6: Differentiation measurements on a 100x100 µm structure with a 632.8 nm Helium-Neon laser line and a 10x magnification. The images (a) and (b) are successively taken (in less than a second), at two different places of the sample, in order to eliminate the background variations (introduce either by the substrate or by the excitation source). The image (c) is the result of the ratio of the images (a) (containing the structure information) over (b) (without structure). The contrast of image (c) is obviously enhanced and the structure appears better. The same process is used for each investigated structure (see Fig. 7).

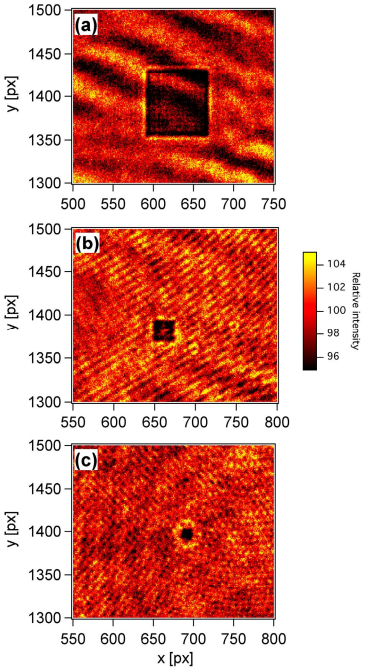

Fig. 7: Images resulting from the process described Fig. 6, on structures of 30x30 µm in (a), of 10x10 µm in (b) and of 5x5 µm in (c).

Indeed, the studied structure may be associated to a Fabry-Perot cavity, as it is a simple glass substrate composed by two parallel faces, with a thickness of 2 mm. Therefore, interferences may occur. We confirmed these oscillations by simulations considering the geometrical and optical parameters of our sample. The refractive index of glass, for λ=632.8 nm, used for the simulations, is taken to be equal to n_s=1.45, and we fixe an index n=1.5 for a small area of 100 nm thick located at one interface of the substrate. By doing so, we attempt to match the experimental conditions as close as possible. The calculation of the transmittance as a function of the incident angle is plotted in Fig. 9. For the given wavelength (632.8nm in our case), the angular spectrum shows oscillations typical of interferences between front and rear side of the substrate. These oscillations are observed in both cases, where the substrate is uniform and where the structure (with n=1.5) is located. The separation distance between two successive fringes depends then only on the thickness of the silica glass. If we now compare the two series of oscillations, we remark slight differences: the location of minima and maxima is nearly the same, but the minimum values are lower of 2.5% for the region of the sample containing the structure (see Fig.9). As in Fig. 9, Fig. 8 shows that the maxima and minima are closely localized at the same angular position (report to Table 1). Moreover, the minimum and maximum values observed from one region to the other follow a 3% deviation.

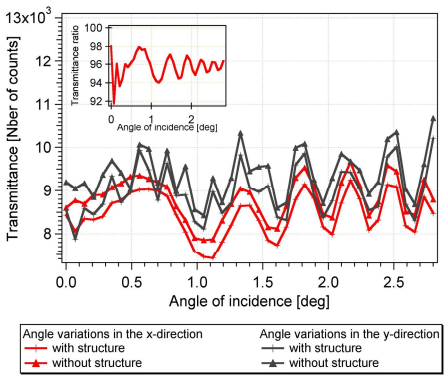

Fig. 8: Transmittance measurements of the 100x100 µm structure, with a $\Delta n=5.10^{-2}$, as a function of the incidence angle for an excitation wavelength of 632.8 nm. The inset gives the ratio of the signal with structure over the one of the background. A good agreement with the calculated curve (See Fig. 9) is observed.

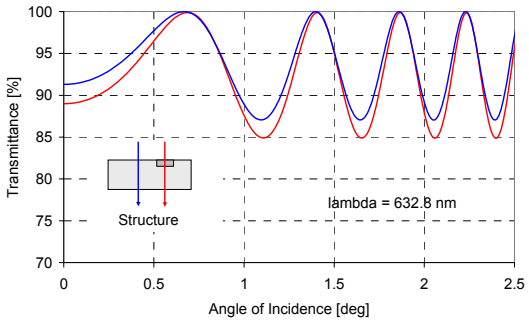

Fig. 9: Numerical transmittance as function of the incident angle without local modifications (blue curve) and with modifications (red curve)

Table 1: Summarize of the angular positions that localize the maxima calculated and measured

θ simulation	0.67	1.40	1.86	2.22	2.54
θ experiment	0.63	1.40	1.89	2.17	2.52

The experimental ratio, given in the inset of Fig. 8, shows oscillations that are typical of the presence of different average refractive index (for both measurements). The mean value is about 96% vs 98% for the theoretical value. This may be explained by the involved fabrication process, namely Ti ions implantation, to create the microstructures. Indeed, it is plausible that for a dose of 2.10^{16} Ti/cm^2, the variation of refractive index is linked to the apparition of a small extinction coefficient (k) in the 10^{-3} range. One can also observe that the oscillations amplitudes seem to decrease with angle from 3% (corresponding to a Δn of 5 10^{-2}) to 1% (corresponding to a fictive Δn of 1.5 10^{-2}). We do not have a physical explanation for this decrease, but we believe that the angular sampling of our experimental study (one measurement each 0.07 degree) becomes insufficient for angles above one degree. Nevertheless, we can conclude that we were able to access to localized Δn thanks to our experimental set up, and to find the expected Δn from our calibrated sample. Some improvements, as explained below and in Section 2, are still needed but the basic principle as been demonstrated. The next step will be to apply this experimental procedure to a sample modified by femtosecond laser trimming.

Finally, in order to optimize the sensitivity on our test samples, we plan to deposit mirrors on both sides to create a resonant structure, as exposed in Section 2. Under the experimental condition (λ=632.8 nm), the optimum envisaged mirrors are stacks of 11 dielectric layers composed by alternated coatings of tantalum pentoxyde (Ta_2O_5) / silica (SiO_2). The resulting transmittance spectra should then be much more resonant as depicted on Fig. 10. The wavelength shift

(Fig. 10 a)) and/or the angle shift (Fig. 10 b)) directly depends on the refractive index modification (5 10^{-2} in our case), and the sharp peak due to the high efficiency of the mirrors is a great help to precisely evaluate the transmittance and therefore determine the associated index variation.

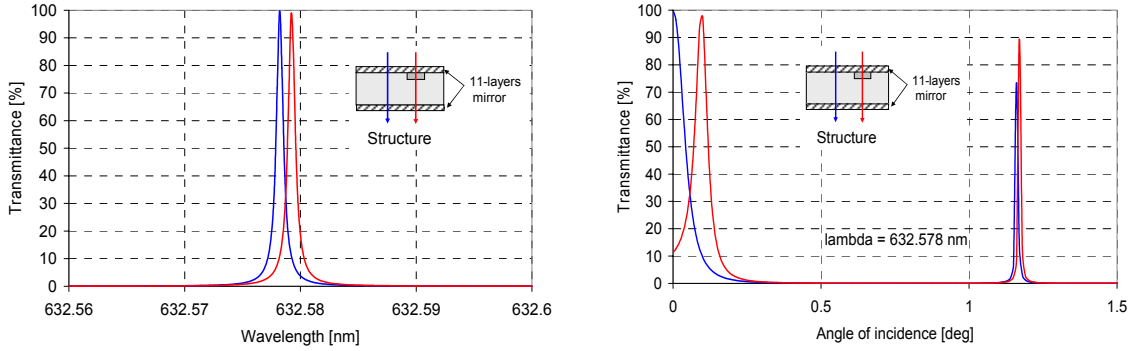

(a) (b)

Figure 10: Numerical predictions of the transmittance versus incident wavelengths (a) and versus incident angles (b) for a resonant structure for λ=632.8 nm. Mirrors of 11 layers are sufficient to obtain sharp peaks and then increase the sensitivity of our apparatus.

5- CONCLUSION

The aim of this work was to elaborate a dedicated experimental way to quantify local variations in the refractive index of a sample modified by femtosecond laser techniques. Therefore, we first numerically anticipated the evaluation in Δn as low as 10^{-4}, spatially localized over regions of 5x5 µm in a wide sample. Indeed, we have shown in Section 2 that by deposing mirrors on both sides of the sample and therefore creating a Fabry-Perot cavity, we could detect very small transmittance variations, corresponding to Δn of at least 10^{-4}, as a function of either the incident wavelength or the incident angle. The optimal cavity was estimated to be composed by two mirrors of 25 thin films.

Hence, in Section 3, we presented the developed experimental setup to measure such spatially localized Δn. We therefore established a differential method based on successive CCD imaging to trace the transmittance variations as function of incident angles, and then access to the Δn modifications (See Section 4). We demonstrated on calibrated samples that we could access to Δn of 10^{-2} on bare samples (with no cavity). Both experimental configurations were necessary to precisely localize and thereafter measure the Δn modifications.

The next steps will be first to implement the Fabry-Perot cavity in order to increase the sensibility of our setup and validate it for Δn of at least 10^{-4} as a function of incident angles and/or incident wavelengths. For this former the use of a lambdameter will allow us to precisely control (in the order of 0.05 pm) the wavelengths changes. Finally, this method is to be applied to femtosecond laser damaged samples where the two experimental configurations will be primary to first of all, localize the damage; second of all, evaluate the Δn in the regions of interest; and third of all, entirely know the characteristics of the final optical component.

ACKNOWLEDGEMENTS

This work was supported by the Agence Nationale de la Recherche (ANR) in the Programme Blanc 2006. The authors would also like to thank Prof. A. Passian at the Oak Ridge National Laboratory USA, and Dr. S. Michel at the Fresnel Institute France, for their fruitful discussions, and David Parrain for his contribution on the experimental set up.

REFERENCES

[1] M.C. Gower, "Industrial applications of laser micromachining," Opt. Exp. **7**, 56-67 (2000)
[2] G.P. Behrmann, M.T. Duignan, "Excimer laser micromachining for rapid fabrication of diffractive optical elements," Appl. Opt. **36**, 4666-4674 (1997)
[3] L. Herbst, R. Paetzel, "High power excimer laser micromachining," Proc. SPIE **6106** Photon Processing in Microelectronics and Photonics V, 50-56 (2006)
[4] J.M. Bovatsek, A.Y. Arai, F. Yoshino, Y. Uehara, "Ultrashort pulse micromachining with the 10- J FCPA fiber laser," Proc. SPIE **6102** Fiber Lasers III: Technology, Systems, and Appications, 1-11 (2006)
[5] C.B. Schaffer, A. Brodeur, J.F. Garcia and E. Mazur, "Micromachining bulk glass by use of femtosecond laser pulses with nanojoule energy," Opt. Lett. **26**, 93-95 (2001)
[6] W.G. Clark, L.A. Walker II, "Micromachining with ultrashort pulses of light," Proc. SPIE **5706** Critical Review: Industrial Lasers and Applications, 69-75 (2005)
[7] X. Yuan, C. Zhu, X. Zhu, G. Zhu, L. Liu, P. Lu, "Practical applications of femtosecond laser micromachining and fabrication," Proc. SPIE **5629** Lasers in Material Processing and Manufacturing II, 284-290 (2005)
[8] A.P. Joglekar, H. Liu, G.J. Spooner, E. Meyhöfer, G. Mourou and A. J. Hunt, "A study of the deterministic character of optical damage by femtosecond laser pulses and applications to nanomachining," Appl. Phys. B**77**, 25-30 (2003)
[9] A.P. Joglekar, H. Liu, E. Meyhöfer, G. Mourou and A.J. Hunt, "Optics at critical intensity: Applications to nanomorphing," PNAS **101**, 5856-5861 (2004)
[10] M.L. Stock, L. Shah, B. Liu, M. Yoshida, F. Yoshino, J. Bovatsek, A. Arai, "Optimized precision micromachining using commercially available high-repetition rate microjoule femtosecond fiber lasers," Proc. SPIE **6108** Commercial and Biomedical Applications of Ultrafast Lasers VI, 136-144 (2006)
[11] K. Miura, J. Qiu, H. Inouye, T. Mitsuyu, and K. Hirao, "Photowritten optical waveguides in various glasses with ultrashort pulses," Appl. Phys. Lett. **71**, 3329-3331 (1997)
[12] M. Will, S. Nolte, and A. Tunnermann, "Single- and multimode waveguides in glasses manufactured with femtosecond laser pulses," Proc. SPIE **4633** Commercial and Biomedical Applications of Ultrafast and Free-Electron Lasers, 99-106 (2002)
[13] A.M. Streltsov and N.F. Borrelli, "Study of femtosecond-laser-written waveguides in glasses," J. Opt. Soc. Am. B **19**, 2496-2504 (2002)
[14] L. Shah, A.Y. Arai, S.M. Eaton, P.R. Herman, "Waveguide writing in fused silica with a femtosecond fiber laser at 522 nm and 1 MHz repetition rate," Opt. Exp. **13**, 1999-2006 (2005)
[15] K. Minoshima, A.W. Kowalevicz, I. Hartl, E.P. Ippen, and J.G. Fujimoto, "Photonic device fabrication in glass by use of nonlinear materials processing with a femtosecond laser oscillator," Opt. Lett. **26**, 1516-1518 (2001)
[16] J.J. Dubowski, "Laser-based technologies for photonic device integration", RIKEN Review **32**, 47-49 (2001)
[17] S. Taccheo, G. Della Valle, R. Osellame, G. Cerullo, N. Chiodo, P. Laporta, O. Svelto, A. Killi, U. Morgner, M. Lederer and D. Kopf, "Er:Yb-doped waveguide laser fabricated by femtosecond laser pulses," Opt. Lett. **29**, 2626-2628 (2004)
[18] Y. Sun, "Interference effect on laser trimming and layer thickness optimization", Proc. SPIE **1598** Lasers in Microelectronic Manufacturing, 91-97 (1991)
[19] W.W. Blooomstein, Laser Trimming: The Competitive Edge in Precision Linear Devices, GSI Lumonics Tech News, http://www.gsilumonis.com/process_online_ordering/pdfs/160.pdf (2001)
[20] A.L. Fehrembach, D. Maystre, and A. Sentenac, "Phenomenological theory of filtering by resonant dielectric gratings," J. Opt. Soc. Am. A **19**, 1136-1144 (2002)
[21] F. Lemarchand, C. Deumié, M. Zerrad, L. Abel-Tiberini, B. Bertussi, G. Georges, B. Lazaridès, M. Cathelinaud, M. Lequime, and C. Amra, "Optical characterization of an unknown single layer: Institut Fresnel contribution to the Optical Interference Coatings 2004 Topical Meeting Measurement Problem," Appl. Opt. **45**, 1312-1318 (2006)
[22] M. Lequime, R. Parmentier, F. Lemarchand, and C. Amra, "Toward Tunable Thin-Film Filters for Wavelength Division Multiplexing Applications," Appl. Opt. **41**, 3277-3284 (2002)